Sergejs Tarasovs

Nonlinear crack problems with application to composites and geomechanics

Summary of Doctoral Thesis

Scientific supervisor:
Dr. habil. sc. ing.
Prof. Vitauts Tamuzs

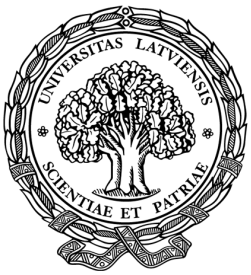

University of Latvia
Institute of Polymer Mechanics

Riga — 2008

Form of promotion work: collection of works

Scientific advisor: Prof. Dr. Habil. Sc. Ing. **Vitauts Tamužs** (University of Latvia)

Reviewers of the work:

1. Senior Researcher, Dr. Habil. Phys. **Donāts Millers**, LU CFI
2. Corr. member of LAS, Professor, Dr. Sc. Ing. **Andris Čate**, RTU
3. Associate Professor, Dr. Phys. **Andris Jakovičs**, LU

Defence of the work is taking place during an open meeting of the Promotion Board in Physics and Astronomy of the University of Latvia

on _____, 2008

at _____ o'clock

in _____, auditorium _____

The work and its summary can be viewed at the Library of the University of Latvia (Riga, Kalpaka blvd. 4) and at the Latvian Academic library (Riga, Rupniecibas str. 10)

Chairman of the specialized Promotion Board in
Physics and Astronomy of the University of Latvia: _____

Šis darbs izstrādāts ar Europas Sociālā fonda atbalstu nacionālās programmas "Atbalsts doktorantūras programmu īstenošanai un pēcdoktorantūras pētījumiem" projekta "Doktorantu un jauno zinātnieku atbalsts Latvijas Universitātē" ietvaros.

This work has been partly supported by the European Social Fund within the National Programme "Support for the carrying out doctoral study programm's and post-doctoral researches" project "Support for the doctoral students and young researchers at University of Latvia".

Abstract

The solution of non-linear problems in mechanics is usually a complex task. It requires much more efforts in analytical and numerical part of the solution (pure analytical solution for most problems is not possible at all). This work comprises solutions of several non-linear problems involving cracks growth and fractures.

In the first part of the work experimental procedure was elaborated in order to find delamination properties of the unidirectional and translaminar-reinforced composites. Bridging law, which can be calculated from experimental data, is found to be important material property. Simple numerical procedure, which uses previously found bridging law, is proposed in order to simulate crack growth in composite laminates.

In second part the three-dimensional mathematical model for analysis of Hot Dry Rock geothermal reservoirs is presented. By utilizing Laplace integral transform and Green's function the solution is reduced to integral equation over the surface of the fracture, which eliminates the need for discretizing the unbounded 3D reservoir. Using presented model temperature and thermally induced stresses can be found anywhere in the reservoir at any time, which makes this model quite efficient in geothermal reservoirs analysis.

1 Introduction

1.1 The aim of the work

The main aims of the work are development of experimental and numerical procedure for analysis of composites delamination and development of three-dimensional numerical model of geothermal reservoirs. To achieve the goal the next tasks should be performed:

- Experimentally analyze the delamination of unidirectional and transversally reinforced composites.
- Show that bridging law is material property and can be used to predict composite delamination.
- Develop a three-dimensional numerical model of geothermal reservoir for prediction of extraction temperature for long time periods.
- Investigate the influence of thermally induced stresses on fracture stability inside reservoir.

1.2 Actuality of the work

Fiber reinforced composites are widely used in modern airplanes, constructions etc. These materials are lightweight and have superior properties. However, heterogeneous structure of such materials is the reason of more complex mechanical behavior, then traditional materials. Composites have many failure modes and therefore new experimental and numerical methods are required to predict the critical loads or durability of structures made from composites. In this work the delamination of fiber reinforced composites in presence of bridging have been studied.

The utilization of geothermal energy is important question and has been studied for many years. One of the primary tasks of geothermal reservoir planning and management is maximization of energy output for long time period. Complex mathematical and numerical models are required to solve this problem. In this work new three-dimensional model for geothermal reservoirs have been developed.

1.3 Scientific novelty and the main results

Experimental technique has been elaborated for measuring delamination properties of unidirectional composites. Similar methodology has been successfully applied to the delamination of transversally reinforced composites.

Numerical procedure is proposed for prediction of delamination process in composites using experimentally obtained data.

New numerical model has been developed for simulation of geothermal reservoirs. The proposed model allows to calculate temperature distribution and thermally induced stresses inside reservoir for long time periods and predict the fracture slip or opening as result of thermal cooling of surrounding rock. The computer program has been developed based on proposed numerical model.

1.4 Approbation of work and the publications

The main results of the work are stated in 6 scientific publications:

1. A. Ghassemi, S. Tarasovs, A. H.-D. Cheng A 3-D study of the effects of thermomechanical loads on fracture slip in enhanced geothermal reservoirs, Int. J. of Rock Mech. & Min. Sci., Vol. 44, 2007, pp. 1132–1148.

2. A. Ghassemi, S. Tarasovs, A. H.-D. Cheng Three-Dimensional Integral Equation Modeling of Injection Induced Thermal Stress in an Enhanced Geothermal Reservoir, *Int. J. Numer. Anal. Meth. Geomech*, 2005, 29, 829–844.

3. A. Ghassemi, S. Tarasovs, A. H.-D. Cheng An integral equation solution for three-dimensional heat extraction from planar fracture in hot dry rock. *Int. J. Numer. Anal. Meth. Geomech.*, 2003, 27, 989–1004.

4. V. Tamuzs, S. Tarasovs Fracture toughness and bridging law of 3D woven composites. Fracture of Polymers, Composites and Adhesives II, 2003, ESIS Publication 32, 515–524.

5. V. Tamuzs, S. Tarasovs, U. Vilks Delamination properties of translaminar-reinforced composites. *Comp. Sci. Technol.*, 2003, 63, 1423–1431.

6. V. Tamuzs, S. Tarasovs, U. Vilks Progressive delamination and fiber bridging modeling in double cantilever beam composite specimens, *Eng. Frac. Mech.*, 2001, 68, 513–525.

The main results of work are reported and discussed at the international scientific and technical conferences in the following reports:

1. A. Ghassemi, S. Tarasovs Fracture slip and opening in response to water injection, Proc. of GRC 2006 Annual Meeting, San Diego, California, USA, September 10–13, 2006.

2. A. Ghassemi, S. Tarasovs A three-dimensional numerical study of fracture slip due to cold water injection in enhanced geothermal reservoirs, Proc. of 41st. U.S. Symposium on Rock Mechanics (USRMS), Golden, Colorado, USA, June 17–21, 2006.

3. A. Ghassemi, S. Tarasovs Fracture slip and opening in response to fluid injection into a geothermal reservoir, Proc. of 31th Workshop on Geothermal Reservoir Engineering, Stanford, California, USA, January 30–February 1, 2006.

4. A. Ghassemi, S. Tarasovs Three-dimensional modeling of Injection Induced Thermal Stresses, Proc. of 6th North American Rock Mechanics Symposium – GulfRocks04, Houston, Texas, June 5–10, 2004.

5. S.Tarasovs Three-dimensional finite-element modeling of fiber bridging in unidirectional composites, 13th International Conference "Mechanics of Composite Materials", Riga, Latvia, May 16–20, 2004, Book of Abstracts, p.186.

6. A. Ghassemi, S. Tarasovs Three-dimensional modeling of Injection Induced Thermal Stresses with an Example from Coso, Proc. of 29th Workshop on Geothermal Reservoir Engineering, Stanford, California, USA, January 26–28, 2004.

7. V. Tamuzs, S. Tarasovs The revised technique of composite delamination tests. Proc. of 6th International Fracture Conference, 10-12 Sep. 2003, Selcuk University Konya, Turkey, 295–304.

8. V.Tamuzs, S.Tarasovs, A.Bogdanovich, J.Singletary Toughness and Bridging Law of 3D Woven Composites, 3rd ESIS TC4 Conference on Polymer and Composites, Les Diablerets, Switzerland, 15–18 September, 2002.

9. V. Tamuzs, S. Tarasovs, U. Vilks Delamination and fiber bridging phenomenon experimental and numerical investigation. Proc. of International Conference on New Challenges in Mesomechanics, Vol. 2, Aalborg University, Denmark, August 26–30, 2002, pp. 605–611.

10. V.Tamuzs, S.Tarasovs, U.Vilks, A.Bogdanovich, J.Singletary Delamination Fracture toughness of 3D Woven Composites, 10th European

Conference on Composite Materials: ECCM-10: Composites for the Future, Brugge, Belgium, June 3–7, 2002, Booklet of Abstracts, p. 3.

11. A. Ghassemi, A. H.-D. Cheng, S. Tarasovs A three-dimensional solution for heat extraction from a fracture in Hot Dry Rock using the boundary element method. Proc. of 27th Annual Workshop "Geothermal Reservoir Engineering", Stanford, California, USA, January 28–30, 2002.

12. V.Tamuzs, S.Tarasovs Modelling of progressive delamination and fiber bridging in DCB specimens, Conference on Mechanics of Composite Materials, Riga, Latvia, June, 2000, Book of Abstracts.

13. V.Tamuzs, S.Tarasovs Fiber Bridging and R-Curve for Interlaminar Fracture of Unidirectional Epoxy-Carbon Composites, ASME Mechanics & Materials Conference, Blacksburg, USA, June, 1999, Book of Abstracts, p. 89.

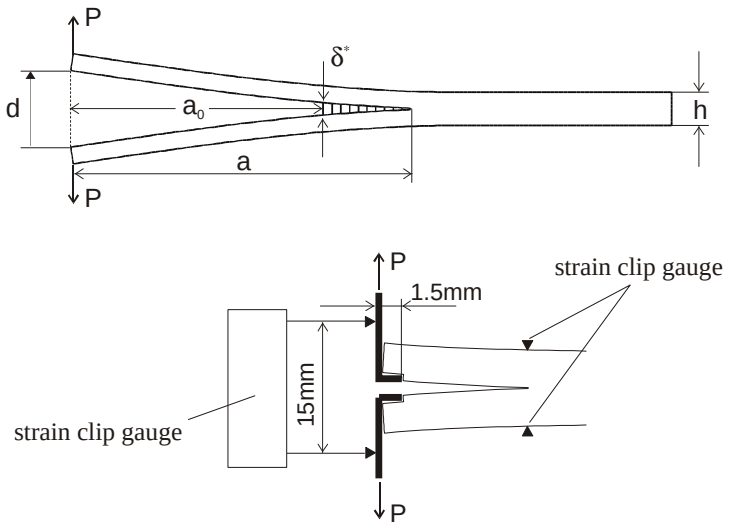

Figure 1: The specimen geometry, loading scheme and measured parameters.

2 Delamination of composites

The resistance to delamination is one of the most important characteristics of laminate and unidirectional composites. One of the interesting features of crack propagation in laminates is extensive fiber bridging, which often can be observed during delamination. This phenomenon can increase the fracture toughness of composites in Mode I up to ten times and therefore it is very important to know how this material property should be measured and how implement it in numerical calculations.

The most popular method of determining the interlaminar fracture toughness in composites is the test of double cantilever beam (DCB) specimens [1]. One of the standard methods to express the ability of material to increase the fracture toughness during crack propagation is so called R-curves - fracture resistance as a function of crack extension.

The concept of a bridging law, traction on a crack faces as a function of crack opening, was introduced in 1992 [2] to characterize the crack growth resistance of a material.

In this work the influence of specimen geometry on R-curves is investigated and scheme of measurements and calculations to predict the resistance of crack propagation in specimens is proposed.

2.1 Energy release rate in DCB specimens

The geometry of a DCB specimen is shown in Fig. 1, where h is the thickness of the specimen, which was varied, a_0 is an initial notch, a is the length of a propagated crack, d is the crack opening under the applied wedge forces P, and δ^* is the crack opening at the tip of the initial notch. The description of the loading and measurement method is given later, in the experimental part.

The energy release rate in a DCB specimen is defined in a usual way:

$$G = -\frac{\partial \Pi}{b \partial a} \tag{1}$$

where b is the width of a specimen, a is the crack length, Π is the potential energy accumulated in the system. For linear elastic system it can be written as:

$$G = \frac{P^2}{2b}\frac{\partial c}{\partial a} \tag{2}$$

where $c = d/P$ is the compliance of the system.

Neglecting the bridging effect, the deflection of an ideal console, with length a and bending stiffness $EI = Ebh^3/12$, under a load P is equal to $a^3P/3EI$. The full opening of the DCB equals the doubled deflection,

$$d = \frac{2a^3P}{3EI} \tag{3}$$

and the compliance is

$$c = \frac{2a^3}{3EI} \tag{4}$$

Using Eqs. (2) and (4), the most popular formula for the DCB is obtained:

$$G(P,a) = \frac{P^2a^2}{EIb} \tag{5}$$

Combining Eqs. (5) and (3), another modified formulae for G can be obtained

$$G(P,d) = \frac{P^2}{EIb}\left(\frac{3EId}{2P}\right)^{2/3} \tag{6}$$

Applying Eqs. (5) and (6) to an ideal isotropic cantilever beam, equal results will be obtained. But, strictly speaking, they are all invalid for DCB specimens, since boundary conditions at the end of cracked part of specimen are not the same as at the clamped end of cantilever beam. As result, the deflection of real specimen for given load and crack extension always will

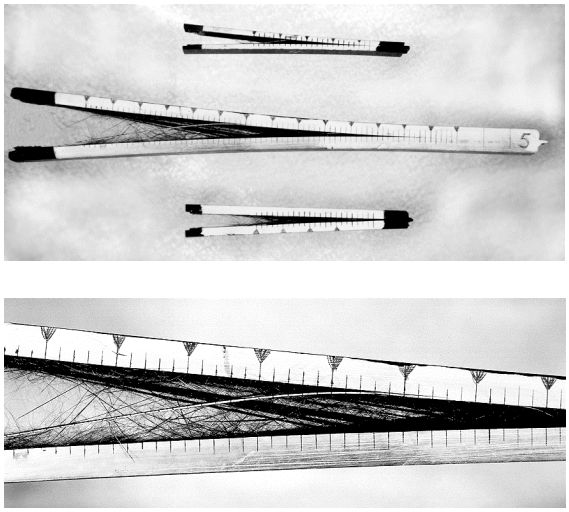

Figure 2: Specimens of three different thicknesses after testing and enlarged bridging zone of a 7-layer specimen.

be greater, then it is predicted by beam theory (3). The deflection is even higher for unidirectional composites, since in Eq. (3) the interlaminar shear is neglected. The error is very big for short crack and diminishes when the crack propagates. Therefore, obtained above formulas will give different results and comparing G calculated directly from finite element analyses with Eqs. (5) and (6), it is found that Eq. (6) performs better even for very short cracks and in presence of large scale bridging.

2.2 Experimental part

The investigated specimens were produced from epoxy/carbon sheets of thickness 1.3 mm. The initial crack was precut by a diamond saw of thickness 0.1 mm and sharpened by a thin blade to extend the initial crack to 25 mm. The width of the cracked specimen b is 11.1 mm. Then the strips of the same material and the same width were glued on both sides of the precracked strip to produce specimens of different total thicknesses, namely 3.93, 6.56 and 9.15 mm corresponding to 3, 5, and 7 layers. The fibers are oriented along the specimen. The length of a specimen is 80 mm for 3-layer and 200 mm for 5- and 7- layer ones.

The material is characterized by the following elastic constants: modulus in the fiber direction $E_1 = 155$ GPa, transverse modulus $E_2 = E_3 = 9$ GPa, shear modulus $G_{12} = 5$ GPa and Poisson ratio $\nu = 0.28$.

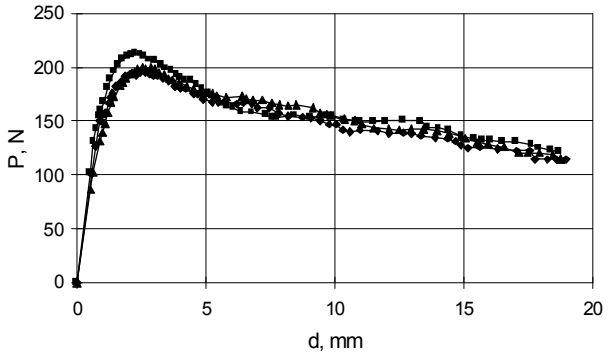

Figure 3: Typical experimental load-displacement curves: $h = 9.15$ mm.

The specimens were loaded by a wedge load under displacement control with a constant speed of 1 mm/min. Seven specimens of thickness 3.93 mm, eight specimens of thickness 6.56 mm and three of thickness 9.15 mm were tested.

The load value was registered by the dynamometer of a MTS testing device, but the crack opening d at the edge of specimens was measured by a strain clip gauge as shown in Fig. 1. The crack opening δ^* at the precrack tip was also measured by second strain clip gauge attached to the top and bottom sides of the specimen. The crack propagation was measured visually. So, the values of P, d, and δ were measured and stored for each crack increment Δa equal to 2 mm.

Extensive bridging was observed during the crack propagation. The specimens with extended and opened cracks are displayed in Fig. 2.

The measured load-displacement curves for 7-layer specimens are shown in Fig. 3. Each point on the curves corresponds to a crack increment $\Delta a = 2$ mm. These values are used later in R-curves calculations (Fig. 4). Energy release rate in all cases was calculated using Eq. (6).

2.3 Bridging law

Calculating the J-integral [3] around the crack tip and along the crack faces with a bridging zone, the following result for the energy release rate is obtained:

$$G = J = \int\limits_S w(\epsilon_{ij})dy - \int\limits_S P_i \frac{\partial u_i}{\partial x} dS = 2\int\limits_a^{a_0} \sigma(x)\frac{\partial u_y}{\partial x}dx + G_0 = \int\limits_0^{\delta^*} \sigma(\delta)d\delta + G_0 \tag{7}$$

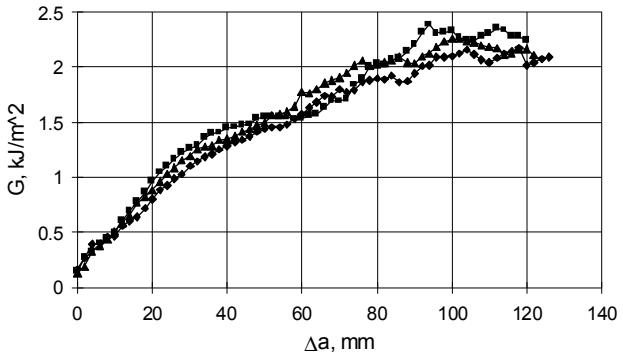

Figure 4: Experimental R-curves for specimens with thickness $h = 9.15$ mm.

from which follows [4, 5] that

$$\sigma(\delta) = \frac{\partial G}{\partial \delta^*} \tag{8}$$

where $\sigma(\delta)$ is traction on a crack faces as a function of crack opening.

For a specimen having a thickness h, the dependences $P(a)$, $d(a)$ and $\delta^*(a)$ are measured, where δ^* is the crack opening at the point where the tip of the initial precrack has been located. With $G(a)$ and $\delta^*(a)$ known, the bridging law $\sigma(\delta)$ is obtained from Eq. (8) and later can be used for numerical simulation of crack propagation in DCB specimens with any thickness.

In Fig. 5a the energy release rate G as a function of the crack opening is plotted for all investigated specimens. The curves for specimens of different thickness almost coincide, taking into account typical scatter of fracture tests. Calculated bridging laws for these specimens are plotted in Fig. 5b.

2.4 Numerical simulation by FEM

The numerical procedure for the simulation of crack propagation taking into account fiber bridging is based on the finite element method with nonlinear "interface elements" embedded along a potential delamination line. The crack propagation is then modeled by introducing an appropriate stress-displacement relationship for the interface elements.

To model the effect of fiber bridging, we will separate the total energy dissipation in a sample into two specific terms associated with the crack tip propagation and with fiber bridging, respectively. We need, therefore, to choose an appropriate stress-displacement relationship for the interface elements, Fig. 6, where σ is the traction across the element and δ is the

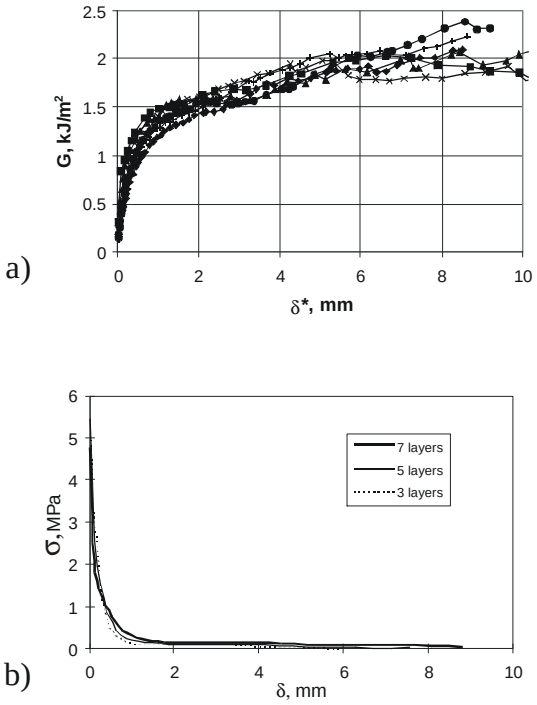

Figure 5: (a) The energy release rate G as a function of the crack opening δ^* at the tip of the initial notch, (b) the experimentally obtained bridging law.

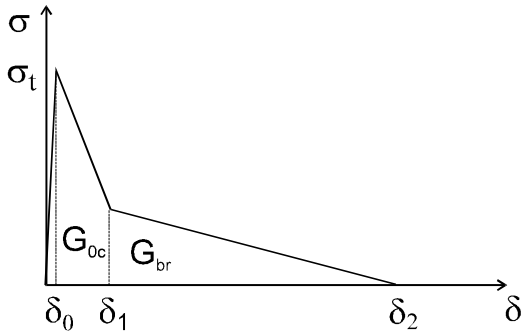

Figure 6: Stress-displacement relationship for interface elements.

opening of crack faces. This work will concentrate on the Mode I fracture only; therefore, the stresses and displacements are both normal to the crack face.

The $\sigma(\delta)$ curve, Fig. 6, comprises three parts corresponding to the displacement intervals $(0, \delta_0)$, (δ_0, δ_1), and (δ_1, δ_2). The first and second part is responsible for the crack initiation and crack tip propagation. When the stress ahead of the crack tip reaches σ_t (the tensile strength of the material) the distance between the elements (interface thickness) is equal to δ_0, and the crack starts to propagate. Behind the crack tip, the stress decrease, and the distance between the crack faces increases up to δ_1. This region is called the "fracture process zone". The numerical tests have shown that the precise value of δ_0 has little effect on the solution, provided that δ_0 is sufficiently small to simulate an initially very stiff interface. The crack opening δ_1 depends on the initial critical fracture energy G_{0c}, which is supposed to be a characteristic of the material. So, the crack opening is chosen such that the area under the curve to the point δ_1 is equal to G_{0c}.

The third part of the stress-displacement relationship (interval from δ_1 to δ_2) depends on the bridging law and the area under the curve represents the energy dissipation due to bridging, G_{br}. As the crack opens, the stress level decreases, being equal to zero at the end of the bridging zone.

Since, for the materials with extensive bridging, the energy release rate during steady state crack propagation, G_{ss}, is up to ten times higher then at the crack initiation, G_c, δ_2 will be many times greater then δ_1. A typical its value for carbon-fiber reinforced plastics is several millimeters. If the actual bridging law for a material is known, it must be utilized when defining the properties of the interface elements.

Using calculated in previous section bridging law of specimen with thickness 9.15 mm as a stress-displacement relationship for the interface elements

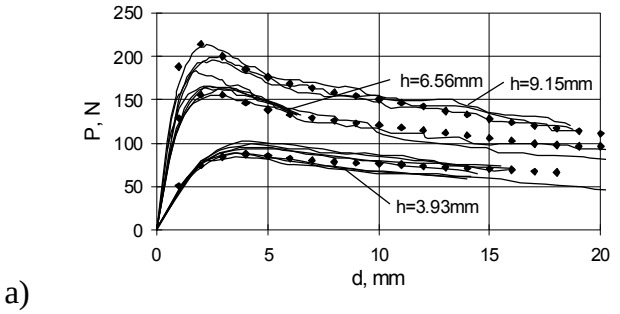

a)

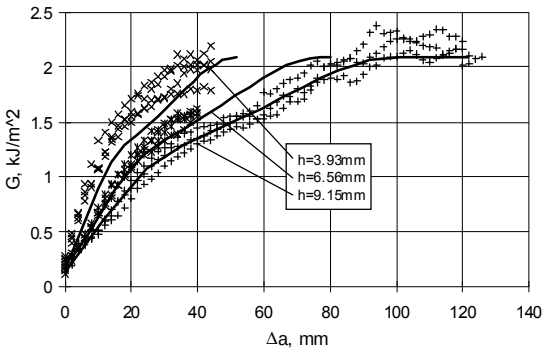

b)

Figure 7: Comparison of the predicted and measured load-displacement and R-curves for different specimen geometries: a) thin lines - experimental curves, dots - prediction; b) predicted R-curves (continuous lines) and a set of experimental R-curves.

in FEM, the load-displacement curves and R-curves are calculated for all tested specimens. The results are summarized in Fig. 7, and a sufficiently good agreement with the experimental data for all specimen geometries is observed.

3 Three-dimensional analysis of geothermal reservoir

Nonlinear fracture mechanics can be applied to the problems of different scales, from small cracks in composites to large fractures in rocks. Hot rocks and geothermal fluids in the subsurface can be an economical source of energy. The temperature in the subsurface rock can rise to 350°C at a depth of 5 km. According to [6], seventy two countries have reported direct utilization of geothermal energy (space heating, industrial use, bathing and swimming, etc.) with total installed capacity 28,268 MW_t. The total annual energy use is 273,372 TJ (75,943 GWh), indicating a 43% increase over 2000. Geothermal electricity is currently being generated in 24 countries with total running capacity approximately 8030 MW_e and and electric energy production is nearly 57,000 GWh [7].

The Hot Dry Rock (HDR) concept of geothermal energy production involves drilling two or more wells into the reservoir to intersect permeable fractures of natural or man-made origin, injecting cold water into one part of the well system, and recovering hot water from the other.

Physical and mathematical models play an important role in the planning and development of geothermal reservoirs. A number of analytical and numerical solutions exist for the prediction of heat extraction from fracture systems in geothermal reservoirs. The physical mechanisms are sometimes complicated and include mechanical, hydraulic, thermal, and chemical effects and their coupling.

The main aim of this work is development of new three-dimensional mathematical model of HDR geothermal reservoir. The model should predict temperature and induced thermal stresses evolution within the reservoir during cold water injection. Fracture opening and slip also will be analyzed using nonlinear fracture mechanincs concepts.

3.1 Fluid flow

Figure 8 gives a schematic view of heat extraction from a hot dry rock system by circulating water through a natural or man-made fracture. The fracture is assumed to be flat, of finite size and with arbitrary shape. The geothermal

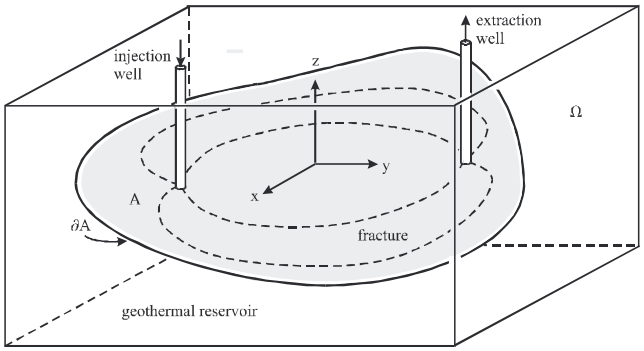

Figure 8: Heat extraction from a planar fracture.

reservoir, on the other hand, is of infinite extent. It is assumed that the geothermal reservoir is impermeable to water and has constant heat conduction properties. The heat storage and dispersion effects in the fracture fluid flow are negligible. The fracture width is small such that the flow in the fracture is laminar and governed by the lubrication flow equation:

$$\nabla_2 p(x,y) = -\frac{\pi^2 \mu}{w^3(x,y)}\,\mathbf{q}(x,y); \qquad x,y \in A \tag{9}$$

where p is the fluid pressure, μ the fluid viscosity, w the fracture width, and A the fracture surface (see Figure 8). Assuming that the fluid is incompressible, the reservoir is impermeable to fluid flow, and the fracture width does not change with time, we can write the fluid continuity equation as

$$\nabla_2 \cdot \mathbf{q}(x,y) = Q\,\delta(x-x_e, y-y_e) - Q\,\delta(x-x_i, y-y_i) \tag{10}$$

where $\nabla_2 \cdot$ is the divergence operator in two dimension. In the above we have considered an injection well located at (x_i, y_i), and an extraction well at (x_e, y_e), both with discharge Q, and δ is the Dirac delta function.

Combining (9) and (10), we obtain the following second order partial differential equation

$$\nabla_2 \cdot \left[w^3(x,y)\,\nabla_2 p(x,y)\right] = \pi^2 \mu\, Q\,[\delta(x-x_i, y-y_i) - \delta(x-x_e, y-y_e)] \tag{11}$$

which is subject to the boundary condition

$$\frac{\partial p}{\partial n} = 0 \qquad \text{on } \partial A \tag{12}$$

where ∂A is the rim of the planar fracture (Figure 8), and n is the outward normal of ∂A. With known fracture width, the above equation can be solved for the pressure distribution in the fracture using finite element method.

3.2 Heat transport

The heat transport occurs both in the geothermal reservoir and the fracture. For the geothermal reservoir, the heat conduction is governed by the three-dimensional diffusion equation:

$$K_r \nabla^2 T_{\mathrm{d}}(x,y,z,t) = \rho_r c_r \frac{\partial T_{\mathrm{d}}(x,y,z,t)}{\partial t}, \qquad x,y,z \in \Omega \tag{13}$$

where ρ_r is the rock density, c_r is the specific heat of rock, K_r is the rock thermal conductivity, Ω represents the infinite geothermal reservoir (Figure 1), and T_{d} is the normalized temperature deficit with a value between zero and one:

$$T_{\mathrm{d}} = \frac{T_0 - T}{T_0 - T_{\mathrm{inj}}} \tag{14}$$

in which T is the temperature, T_0 is the initial rock temperature, and T_{inj} is the temperature of injected water.

For heat transport in the fracture the governing equation is

$$\mathbf{q}(x,y) \cdot \nabla T_{\mathrm{d}}(x,y,0,t) = \frac{2K_r}{\rho_w c_w} \left. \frac{\partial T_{\mathrm{d}}(x,y,z,t)}{\partial z} \right|_{z=0^+} \tag{15}$$

where ρ_w is the water density, c_w is the specific heat of water.

Prior to the heat extraction operation, the temperature of the rock and the fracture fluid is assumed to be a constant, $T(x,y,z,0) = T_0$, and at the injection point $(x_i, y_i, 0)$ the temperature equals that of the injected water: $T(x_i, y_i, 0, t) = T_{\mathrm{inj}}$. The extraction temperature $T(x_e, y_e, 0, t)$ is unknown. The initial and the boundary condition can be expressed in terms of T_{d}:

$$T_{\mathrm{d}}(x,y,z,0) = 0; \qquad T_{\mathrm{d}}(x_i, y_i, 0, t) = 1 \tag{16}$$

To facilitate the treatment of the time variable, we apply Laplace transform to the above equations and obtain

$$K_r \nabla^2 \widetilde{T}_{\mathrm{d}}(x,y,z,s) = s\rho_r c_r \widetilde{T}_{\mathrm{d}}(x,y,z,s) \tag{17}$$

$$\mathbf{q}(x,y) \cdot \nabla \widetilde{T}_{\mathrm{d}}(x,y,0,s) = \frac{2K_r}{\rho_w c_w} \left. \frac{\partial \widetilde{T}_{\mathrm{d}}(x,y,z,s)}{\partial z} \right|_{z=0^+} \tag{18}$$

$$\widetilde{T}_{\mathrm{d}}(x_i, y_i, 0, s) = \frac{1}{s} \tag{19}$$

where the wiggle overbar denotes the Laplace transform, and s is the transform parameter. Equations (17)–(19) form a complete solution system.

The system of Equations (17)–(18) is defined in three spatial dimensions. It has been demonstrated that by utilizing Green's function of three-dimensional diffusion equation, the solution system can be reduced to a two-dimensional integral equation. For the temperature on the fracture surface ($z = 0$) we obtain

$$\widetilde{T}_d(x,y,0,s) = -\frac{\rho_w c_w}{4\pi K_r}\int_A \left[\mathbf{q}(x',y')\cdot\nabla\,\widetilde{T}_d(x',y',0,s)\right] \frac{1}{r}\exp\left(-\sqrt{\frac{\rho_r c_r s}{K_r}}\,r\right)\,dx'dy'; \qquad x,y\in A \tag{20}$$

where $r = \sqrt{(x-x')^2+(y-y')^2}$.

The general scheme for solving the system represented by (20) involves discretizing an arbitrary shaped fracture surface into a number of elements defined by a total of $n+1$ nodes. An unknown temperature deficit $\widetilde{T}_d^i$ is associated with each node, with the exception of the injection point, where $\widetilde{T}_d = 1/s$ is the imposed boundary condition. As a result, there are n unknown discrete temperatures. Equation (20) is then applied to the n nodes by selecting in turn their nodal locations as the base point. This produces n equations to solve for the n unknowns.

The area integration in (20) is performed element by element with reference to local co-ordinates (η,ξ):

$$\widetilde{T}_d(x,y,s) = \frac{-\rho_w c_w}{4\pi K_r}\sum_{m=1}^{n_e}\int_{A_m}\left[q_x(\eta,\xi)\frac{\partial\widetilde{T}_d(\eta,\xi,s)}{\partial\eta} + q_y(\eta,\xi)\frac{\partial\widetilde{T}_d(\eta,\xi,s)}{\partial\xi}\right]\frac{1}{r}\exp\left(-\sqrt{\frac{\rho_r c_r s}{K_r}}\,r\right)\,d\eta d\xi \tag{21}$$

The values of q_x, q_y, $\partial\widetilde{T}_d/\partial\eta$, and $\partial\widetilde{T}_d/\partial\xi$ within the element are interpolated from their nodal values based on bilinear shape functions. The resulting linear system contains the nodal values of temperature as unknowns. An LU decomposition scheme is then employed to solve the matrix. The solution obtained above is in the Laplace transform domain. It is necessary to transform the solution back into the time domain. This is achieved by using an approximate Laplace inversion method. The widely used Stehfest method [8] is adopted for this purpose.

3.3 Thermally induced stresses

Let us assume that the reservoir rock is isotropic, homogeneous and elastic. The change in temperature $\Delta T = T - T_0$ can be related to the Goodier

thermoelastic displacement potential Φ through this Poisson equation:

$$\nabla^2 \Phi = m\, \Delta T \tag{22}$$

where

$$m = \frac{(1+\nu)\alpha_T}{(1-\nu)} \tag{23}$$

is the thermoelastic constant, α_T is the coefficient of linear thermal expansion and ν is the Poisson ratio. Here we recall the definition

$$\mathbf{u} = \nabla \Phi \tag{24}$$

where $\mathbf{u}$ is the displacement vector.

Consider an instantaneous heat source of unit intensity located at (x', y', z') and at time t'. Solving for the displacement potential defined in (22), we obtain Green's function

$$\Phi^*(x-x', y-y', z-z', t-t') = -\frac{m}{4\pi\rho_r c_r R}\, \mathrm{erf}\left(\frac{R}{\sqrt{\vartheta}}\right) \tag{25}$$

where

$$\vartheta = 4\kappa(t-t') \tag{26}$$

and

$$\kappa = \frac{K_r}{\rho_r c_r} \tag{27}$$

Now, for a distribution of heat sources with the intensity $\mu(x, y, t)$ over the fracture surface A, the resultant displacement potential at any given location and time can be obtained from the Duhamel's principle of superposition:

$$\Phi(x, y, z, t) = \int_0^t \int_A \mu(x', y', t')\ \Phi^*(x-x', y-y', z, t-t')\ dx'dy'dt' \tag{28}$$

Similar to (20), the above equation involves the integration over the finite fracture surface only. To facilitate the treatment of time, we apply Laplace transform to (28) and obtain

$$\widetilde{\Phi}(x, y, z, s) = \int_A \widetilde{\mu}(x', y', s)\ \widetilde{\Phi}^*(x-x', y-y', z, s)\ dx'dy' \tag{29}$$

where

$$\widetilde{\Phi}^*(x-x', y-y', z, s) = -\frac{m}{4\pi s\rho_r c_r R}\left[1 - \exp\left(-\sqrt{\frac{s}{\kappa}}R\right)\right] \tag{30}$$

We realize that the source intensity $\widetilde{\mu}$ is just the cooling fluid-induced temperature flux on the fracture surfaces, and

$$\widetilde{\mu} = -2K_r \left. \frac{\partial \widetilde{T}}{\partial z} \right|_{z=0^+} \tag{31}$$

Utilizing the heat transport equation (18) in the above and substituting it into (31), we obtain

$$\begin{aligned} \widetilde{\Phi}(x,y,z,s) &= \frac{m\,\rho_w\,c_w}{4\pi s \rho_r c_r} \int_A \left[\mathbf{q}(x',y') \cdot \nabla \widetilde{T}(x',y',0,s) \right] \\ &\quad \left[\frac{1}{R_1} - \frac{1}{R_1} \exp\left(-\sqrt{\frac{s}{\kappa}} R_1 \right) \right] \, dx'\, dy' \end{aligned} \tag{32}$$

The right-hand side of the above equation consists entirely of known quantities, because the fluid flow and the temperature in the fracture have been obtained from the previous stage of solution based on (20).

The stresses are related to the displacement potential by the following formula

$$\widetilde{\sigma}_{ij} = 2G \left(\frac{\partial^2 \widetilde{\Phi}}{\partial x_i \partial x_j} - \delta_{ij} \nabla^2 \widetilde{\Phi} \right) \tag{33}$$

With Eq. (33) the thermally induced stresses can be found anywhere in the geothermal reservoir.

3.4 Fracture Slip

In this work, the fracture opening and slip are determined using a 3D elastic displacement discontinuity method. The displacement discontinuity method is an indirect boundary element method which is based on the fundamental solution of a point displacement discontinuity (DD) in an infinite elastic or poroelastic medium. This technique has been used extensively in mining and hydraulic fracturing.

The tractions on the fracture surface due to displacement discontinuities can be written in form of integral equation of the first kind:

$$\sigma_{ij}(x) = \int_\Gamma \sigma^*_{ijkn}(\xi, x)\ \Delta D_{kn}(\xi)\ d\Gamma \tag{34}$$

with known values of σ_{ij} and unknown values of ΔD_{kn}. The kernel σ^*_{ijkn} represents the effect of a point displacement discontinuity at point ξ on the tractions at point x. A general analytical solution of this equation is not

possible, therefore it is necessary to solve it numerically by transforming the integral equation into a system of algebraic equations. The fracture surface is divided into number of elements and induced stresses on element "m" due to a constant spatial distribution of normal and shear DD's on element "r" are given by:

$$\sigma_{ij}^{m}(x) = S_{ijkn}^{rm}(\xi, x)\Delta D_{kn}^{r}(\xi) \tag{35}$$

It should be noted, that for a planar fracture shear stresses depend on both shear components of displacement discontinuity while the normal stress components depend only upon the normal component of DD. Thus, the σ_{zz} stress component for the elements are independent of σ_{xz} and σ_{yz}; therefore, they can be solved separately. Applying Eq. (35) for normal and shear stress components and summarizing the influence coefficients of all elements, two systems of algebraic equations are formed for N closure and $2N$ ride unknowns:

$$\sigma_{zz} = K_{zz}D_{zz} \tag{36}$$

$$\begin{bmatrix} \sigma_{xz} \\ \sigma_{yz} \end{bmatrix} = \begin{bmatrix} K_{xx} & K_{xy} \\ K_{yx} & K_{yy} \end{bmatrix} \begin{bmatrix} D_{xz} \\ D_{yz} \end{bmatrix} \tag{37}$$

where K is the matrix of influence coefficients; K_{zz} represents the normal stresses due to normal DD's in the z-direction, K_{xy} represents the shear stress in the x-direction due to shear DD's in the y-direction, and so on.

When the fracture remains open, these equations can be solved in a simple manner. In this case, the slip corresponds to the magnitude of shear displacement discontinuities. However, a different approach is needed when the fracture is closed. In this case, the fracture is modeled using a rigid perfectly plastic Mohr-Coulomb element. The shear strength of the Mohr-Coulomb element is given by:

$$\tau = c_0 + \sigma_n \tan\phi_{ef} = c_0 + \sigma_n \tan(\phi_{in} + \varphi_{dil}) \tag{38}$$

where ϕ_{ef} is the effective friction angle of the joint/fault surface, ϕ_{in} is intrinsic friction angle, φ_{dil} is dilation angle, σ_n is the compressive stress acting on the fracture surface and c_0 is the cohesion. The standard Coulomb friction model assumes that no relative motion occurs if the equivalent shear stress (Eq. 39) is less than the critical stress, predicted by Eq. (38).

$$\tau_{eq} = \sqrt{\sigma_{xz}^2 + \sigma_{yz}^2} \tag{39}$$

The fracture aperture is affected by the amount of shear displacement and is equal to:

$$a = U\tan(\varphi_{dil}) \tag{40}$$

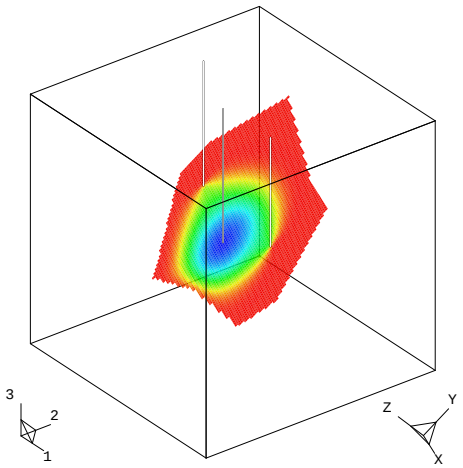

Figure 9: Inclined fracture with one injection well and two production wells.

where φ_{dil} is dilation angle and $U = \sqrt{D_{xz}^2 + D_{yz}^2}$.

To set up the system of equations for a given problem, the in-situ stresses and hydraulic pressure are applied in the initial solution step. Then thermal load is applied incrementally, Then, an iterative solution process is used taking into account Mohr-Coulomb friction criterion.

This mathematical model was implemented in a computer program for the solution of temperature and stresses in cold-water injection into hot fracture problem. Program has a user-friendly graphical interface to set up the properties of reservoir and for solution visualization. The three-dimensional plot of inclined fracture with one injection well and two production wells is presented in Figure 9. The gray shaded area in plot represents the rock cooled zone due to cold water injection in geothermal reservoir.

Figures 10–14 show temperature distribution, thermally induced stresses and fracture opening/slip for inclined fracture problem (Figure 9) after 3 month of operation. Input parameters are shown in Table 1. It was assumed, that fracture is located at a depth of 2330 m with an in situ stress of σ_v = 60.13 MPa, $\sigma_{h\,\min}$ = 34.81 MPa, $\sigma_{H\,\max}$ = 50.88 MPa, and a water pressure of 25 MPa. Results show, that fracture opening and slip are strongly depend on thermally induced stresses and it should be taken into account in geothermal reservour analysis.

E	Young's modulus	65.0	GPa
ν	Poisson's ratio	0.185	
ρ_r	rock density	2650	$\mathrm{kg/m^3}$
ρ_w	water density	1000	$\mathrm{kg/m^3}$
c_r	rock heat capacity	790	J/(kg K)
c_w	water heat capacity	4200	J/(kg K)
κ	thermal diffusivity	5.1×10^{-6}	$\mathrm{m^2/sec}$
α_T	rock linear thermal expansion coefficient	8.0×10^{-6}	1/K
Q	injection rate	40	ℓ/sec
T_R	rock temperature	180	°C
T_{inj}	injection water temperature	30	°C
w	initial average fracture aperture for flow	10^{-3}	m

Table 1: Input parameters.

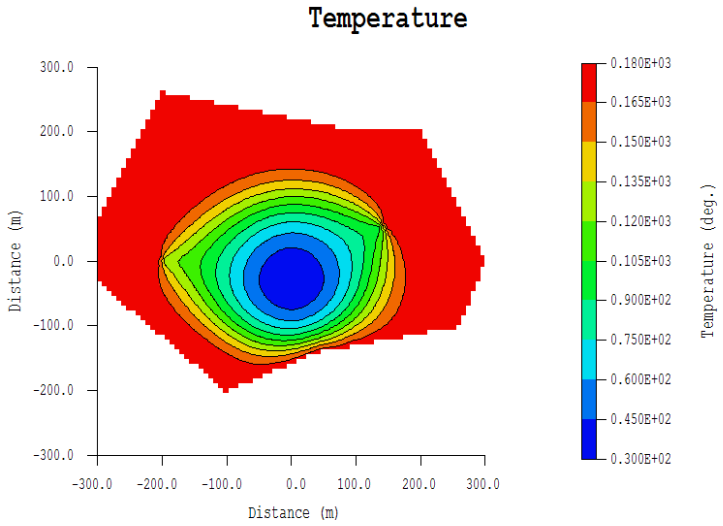

Figure 10: Temperature distribution in the fracture after 3 months of operation.

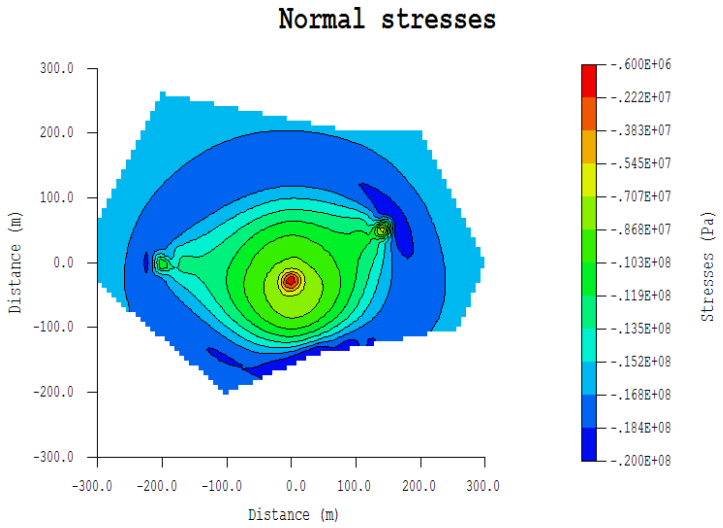

Figure 11: Normal stresses acting on the fracture plane after applying the in-situ stresses, pressure, and thermal stresses.

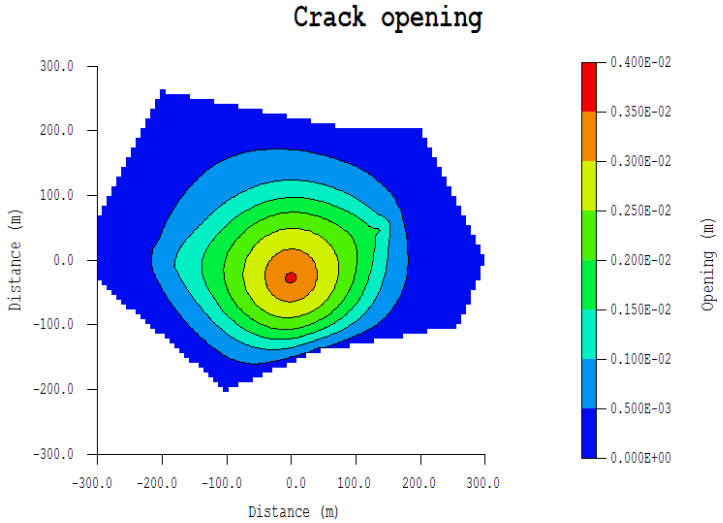

Figure 12: Crack opening after 3 months of injection (maximum opening is 4 mm).

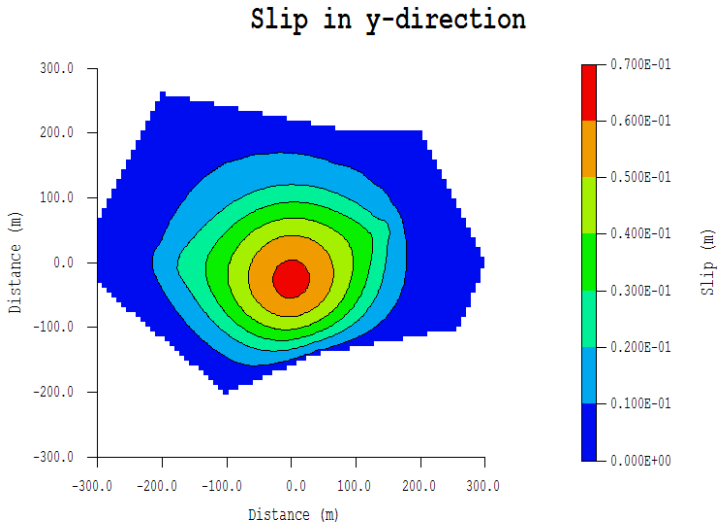

Figure 13: Slip in the y-direction.

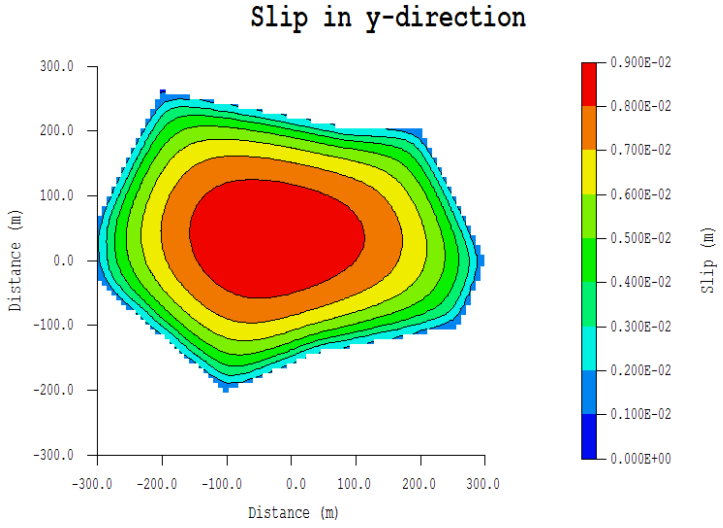

Figure 14: Shear slip in the y-direction in the absence of thermal stresses.

4 Conclusions

Nonlinear fracture mechanics methods have been applied to the different problems. Experimental procedure has been developed for determination of unidirectional composite intralaminar fracture toughness. The additional parameter crack opening displacement at the initial precrack tip (ICOD) was measured to obtain the bridging law, which is independent on the geometry of specimen. Similar methodology was applied to translaminar-reinforced composites.

- It was demonstrated, that bridging law is characteristics of material and therefore can be used to predict fracture propagation in different situations.
- Simple numerical procedure has been used to simulate crack propagation in unidirectional composites, using experimentally calculated bridging law.
- It is recommended to use the graphs G_{IC} vs. ICOD, instead of traditional R-curves (G_{IC} vs. Δa) for characterization of delamination fracture resistance of composite with extensive bridging.
- Presence of transverse fibers does not delay damage initiation, but resistance to crack propagation is greatly improved for such materials.

A 3D boundary element model for heat extraction/thermal stress has been coupled with a 3D elastic displacement discontinuity method to investigate the fracture opening and slip in response to pressure and cooling of the rock under a given in-situ stress field. Using this approach, the effects of each mechanism on rock stress and fracture slip have been estimated. As results of numerical simulation of heat extraction from geothermal reservoir it has been found that:

- presented in this work integral equation scheme offer a fast and numerically efficient method to analyze temperature distribution inside geothermal reservoir;
- three-dimensional heat conduction mechanism should be taken into account to estimate energy output of geothermal reservoir during long-term operation;
- analysis of thermally induced stresses show that not only tensile stresses develop due to the cooling, but also compressive stresses are generated in the range just outside of the cooled zone;

- the results of displacement analysis indicate that under typical field conditions, a substantial increase in fracture slip is observed when thermal stresses are taken into account. The amount of slip would depend on the rock properties, in-situ stress, pressure, injection rate, and degree of cooling. This slip can be accompanied by seismicity; it would also result in redistribution of stresses in the rock mass and may induce slip and seismicity elsewhere in the reservoir.

References

[1] ASTM D 5528–94a. Standard test method for mode I interlaminar fracture toughness of unidirectional fiber-reinforced polymer matrix composites. Annual Book of ASTM Standards, American Society for Testing and Materials, Philadelphia.

[2] Suo Z., Bao G. and Fan B. (1992) Delamination R-curve phenomena due to damage. *J.Mech.Phys.Solids.* 40,1.

[3] Rice J.R. (1968) A path independent integral and the approximate analysis of strain concentrations by notches and cracks. *J. Appl. Mech.*, 35, 379–386.

[4] Li V.C., Chan C.M., Leung K.Y. (1987) Experimental determination of the tension-softening relations for cementitious composites. *Cement and Concrete Research*, 17, 441–452.

[5] Bao G., Suo Z. (1992) Remarks on crack-bridging concepts. *Applied Mech. Rev.*, 45, 355–366.

[6] Lunda, J.W., Freeston, D.H. and Boyd, T.L Direct application of geothermal energy: 2005 Worldwide review, *Geothermics,* **34** (2005), 691–727.

[7] Bertani, R. World geothermal power generation in the period 2001–2005, *Geothermics,* **34** (2005), 651–690.

[8] Stehfest H. Numerical inversion of Laplace transforms. *Communication ACM* 1970; **13**: 47–49 and 624.